SOFT ROBOTICS
Volume 00, Number 00, 2018
© Mary Ann Liebert, Inc.
DOI: 10.1089/soro.2017.0085

SoRo
Soft Robotics

ORIGINAL ARTICLE

Understanding Fish Linear Acceleration Using an Undulatory Biorobotic Model with Soft Fluidic Elastomer Actuated Morphing Median Fins

Li Wen,[1] Ziyu Ren,[1] Valentina Di Santo,[2] Kainan Hu,[1] Tao Yuan,[1] Tianmiao Wang,[1] and George V. Lauder[2]

Downloaded by Ucsb Libraries University of California Santa Barbara from www.liebertpub.com at 04/10/18. For personal use only.

Abstract

Although linear accelerations are an important common component of the diversity of fish locomotor behaviors, acceleration is one of the least-understood aspects of propulsion. Analysis of acceleration behavior in fishes with both spiny and soft-rayed median fins demonstrates that fin area is actively modulated when fish accelerate. We implemented an undulatory biomimetic robotic fish model with median fins manufactured using multimaterial three-dimensional printing—a spiny-rayed dorsal fin, soft-rayed dorsal/anal fins, and a caudal fin—whose stiffnesses span three orders of magnitude. We used an array of fluidic elastomeric soft actuators to mimic the dorsal/anal inclinator and erector/depressor muscles of fish, which allowed the soft fins to be erected or folded within 0.3 s. We experimentally show that the biomimetic soft dorsal/anal fin can withstand external loading. We found that erecting the soft dorsal/anal fins significantly enhanced the linear acceleration rate, up to 32.5% over the folded fin state. Surprisingly, even though the projected area of the body (in the lateral plane) increased 16.9% when the median fins were erected, the magnitude of the side force oscillation decreased by 24.8%, which may have led to significantly less side-to-side sway in the robotic swimmer. Visualization of fluid flow in the wake of median fins reveals that during linear acceleration, the soft dorsal fin generates a wake flow opposite in direction to that of the caudal fin, which creates propulsive jets with time-variant circulations and jet angles. Erectable/foldable fins provide a new design space for bioinspired underwater robots with structures that morph to adapt to different locomotor behaviors. This biorobotic fish model is also a potentially promising system for studying the dynamics of complex multifin fish swimming behaviors, including linear acceleration, steady swimming, and burst and coast, which are difficult to analyze in freely swimming fishes.

Keywords: hydrodynamics, biorobotic fish, soft morphing fins

Introduction

A KEY CHARACTERISTIC of the locomotor design of fishes is the presence of median fins. The dorsal, anal, and caudal fins are all midline structures that are actively used by fishes during locomotion as fluid control surfaces. These fins possess intrinsic musculature, distinct from myotomal (or body) muscles that power body undulation, that allows control over both fin surface area and conformation.[1–7] Understanding how fish use median fins is important for evaluating the diversity of locomotor behaviors in fishes, including the variety of maneuvering activities that are part of the normal swimming repertoire. For example, the spiny and soft dorsal and anal fins can be erected or folded down during swimming to alter the laterally projected body surface area, and changes also occur in the surface area of the dorsal and anal fin regions supported by flexible fin rays. Many teleost fishes possess distinct regions of median fins, with an anterior portion (especially of the dorsal fin) supported by spines, while the membrane of the posterior fin region is supported by flexible fin rays.[8–11]

Among the diversity of maneuvering behaviors in fishes, which include fast start escape responses, turning, backward

[1]School of Mechanical Engineering and Automation, Beihang University, Beijing, China.
[2]The Museum of Comparative Zoology, Harvard University, Cambridge, Massachusetts.

Downloaded by Ucsb Libraries University of California Santa Barbara from www.liebertpub.com at 04/10/18. For personal use only.

locomotion, rapid burst and coast swimming, and linear acceleration, the latter is the least understood aspect of swimming (Fig. 1A). Although Tytell[12] studied the kinematics and hydrodynamics of routine linear accelerations of eels (*Anguilla rostrata*), almost all studies of fish locomotion have focused on other types of fish locomotor behavior. In part, this is likely due to the considerable difficulty in reliably and repeatedly eliciting linear accelerations from freely swimming fishes, and the challenges of generating a replicated data set in which fish accelerate with a variety of known values. From our observation on a largemouth bass (*Micropterus salmoides*) (Fig. 1B, C), we found a significant change in median fin area during the linear acceleration at different time instants (Fig. 1D).[11]

A robotic model with morphing median fins that allows control over fin surface area and also the ability to precisely generate linear accelerations that vary in magnitude would be a valuable tool for exploration of this aspect of unsteady fish locomotor behavior.

Fish-inspired biorobotic flexible models have attracted growing attention from mathematicians,[16] fluid engineers,[17] roboticists,[18,19] and biologists[20,21] interested in studying the principles underlying unsteady locomotion in aquatic animals. Previous studies have included bioinspired mechanisms that produce movements similar to swimming fishes to mimic pectoral fin,[22] caudal fin,[23] and undulatory body locomotion.[24] More recent studies have used soft actuators and smart materials to mimic fish-like locomotion. For example, Marchese *et al.*[25] have developed a soft robotic fish body powered by fluidic actuators that is capable of performing a C-start escape response. Kim *et al.*[26] have developed robotic pectoral fins with a shape memory alloy that can generate undulation motions similar to a ray's. Jusufi *et al.*[27] used pneumatic actuators attached to a flexible foil to study how undulatory locomotion of a simple model fish body is altered by changing the level of cocontraction of right and left side actuators.

From the biomimetic perspective, both fin movements and body deformation should be included when characterizing the hydrodynamic function of a bioinspired robotic fish. Creating a biologically analogous robotic fish with median fins is a considerable challenge because it requires fabricating multiple engineered fins whose Young's modulus ranges between 10^5 and 10^9 Nm^{-2},[16,28] and then actuating and controlling the undulatory body and multiple individual fin elements that make up the entire system.

Development of a fish robotic system that allows controlled analysis of acceleration behaviors also has the potential of contributing to understanding different behaviors exhibited by freely swimming fishes. For example, changing fin areas during steady swimming and during unsteady behaviors such as turning and acceleration are commonly observed, as are differences in kinematics between spiny and soft-rayed dorsal fins,[9,10] and the increase in body yaw (side to side) motion as fishes accelerate.[29] However, understanding the effects of such fin or body motions on swimming performance and the balance between thrust and drag forces is very difficult in living fishes. Using a robotic model system in which fin surface areas and body motions can be altered and effects on swimming performance quantified provides a valuable tool by which robotics can contribute to understanding the complex and multifactorial swimming behaviors in live fishes.

In this study, we present an engineered robotic fish that includes morphing flexible median fins that can be actively controlled along with control of undulatory body motion and the swimming acceleration profile. Two key questions underpinned our research. First, can we design and fabricate a biomimetic robotic fish with median fins that can morph into different shapes, and that accurately reflect fish median fin function? Second, how does altering median fin surface area affect linear acceleration swimming performance of the robotic fish? To answer these questions, we need to fabricate

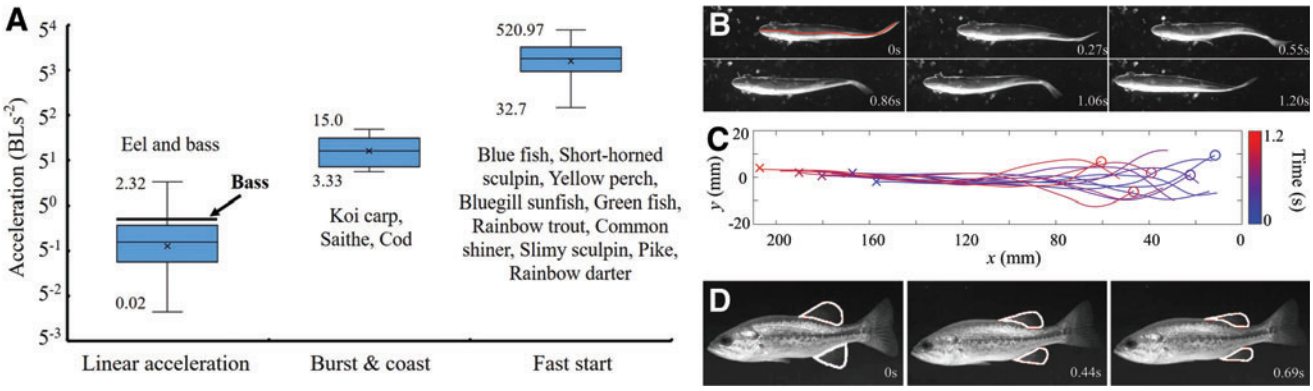

FIG. 1. Linear acceleration in live fish. **(A)** The range in acceleration of the three typical types of unsteady swimming behaviors is given in BL/s^2. Species beneath each box plot are listed in order of increasing acceleration values. Among the three kinematic modes—linear acceleration,[12] burst and coast (also called ''kick and glide''),[13,14] and fast-start[15] (including C-starts and S-starts)—linear acceleration in fish is the least understood. **(B)** Representative image sequence of a largemouth bass (*Micropterus salmoides*) performing linear acceleration at 0.17 BL/s^2. The body midlines were extracted with a time interval of 0.27 s. Frames from $t = 0$ s to 1.2 s shows a series of tail beats of four cycles during linear acceleration. **(C)** Body midline profiles during linear acceleration are illustrated. The snout position is indicated by ''x,'' and the tail position is denoted by ''o.'' **(D)** Representative image sequences of the bass in the lateral view, the soft-rayed dorsal/anal fins are outlined with *solid white* lines. Fin area changed from 732 mm^2 ($t = 0$ s) to 381 mm^2 ($t = 0.69$ s) during linear acceleration—a decrease of 47.9% in total area of the soft-rayed dorsal/anal fins. BL, body length. Color images available online at www.liebertpub.com/soro

Downloaded by Ucsb Libraries University of California Santa Barbara from www.liebertpub.com at 04/10/18. For personal use only.

synthetic median fins based on the morphological design principles of bony fishes and test the hydrodynamic function of the fins on an undulatory robotic model that could move like a fish. To our knowledge, no previous study has either reported on ''morphing'' fins attached to a fish-inspired underwater robot, or tested the effects of morphing fin states on hydrodynamic performance under self-propelled swimming conditions.

For this study, we first used synchronized ventral and lateral high-speed cameras to examine linear acceleration behavior and median fin conformation in largemouth bass (*M. salmoides*). Then, we designed and fabricated a spiny-rayed dorsal fin, soft-rayed dorsal/anal fins, and a caudal fin, which were manufactured using multimaterial three-dimensional (3D) printing. These biomimetic fins were actuated by fluidic elastomeric soft actuators that mimicked the functions of the dorsal/anal erector/depressor muscles of live fish, and were also designed to have lightweight, compliant features that could withstand impacts and resist fluid loading. We then attached the fins at the proper positions to a fish-like robotic undulatory platform with a rigid skeleton and controlled the acceleration profile of the entire platform of actuated median fins plus undulatory body. Finally, we measured the speed, linear acceleration, lateral and thrust forces, and wake flow patterns of this biorobotic fish while varying fin conformation under self-propelled swimming conditions on a custom-designed experimental system.[24,30,31]

Materials and Methods

Largemouth bass (*M. salmoides*) were collected in Massachusetts (United States) and housed in Harvard University aquaria at room temperature. Animal experiments were conducted in a closed circuit flow tank with a 25-cm-wide, 25-cm-deep, and 80-cm-long working section. Bass, mean body length (BL) of 15 cm, were confined to the working section using plastic grids as in our previous research.[9] To record the linear acceleration of bass, animals were gently maneuvered into position in front of the cameras. After a period of steady swimming in the flow (at both 1 BL/s and 2 BL/s in our study), bass would periodically and voluntarily accelerate linearly in response to a stimulus introduced behind them. Linear acceleration was filmed as fish began from steady locomotion at these two flow speeds with synchronized ventral and lateral high-speed cameras (Photron PCI-1024, 1 megapixel resolution) at 1000 fps. The research was conducted under the approved Institutional Animal Care and Use protocol #20-03 at Harvard University.

To investigate the effects of morphing fin states on hydrodynamics during linear acceleration, we implemented a biomimetic undulatory fish robotic model with median fins—a biomimetic spiny-rayed dorsal fin, soft-rayed dorsal/anal fins, and a caudal fin—based on the morphological design of perch-like bony (teleost) fishes that possess dorsal fins with both spines and flexible fin rays.

The spiny dorsal fin of most teleost fish species can be elevated and depressed by erector/depressor muscles.[32] To mimic this rotational motion of a spiny dorsal fin (Fig. 2A), we used a four-bar linkage mechanism that translates the linear movement of a fiber-reinforced cylindrical soft actuator into rotational movement for five fin rays connected by a membrane (Fig. 2B). The fiber-reinforced cylindrical soft actuator (Supplementary Fig. S1; Supplementary Data are available online at www.liebertpub.com/soro), which activates by being inflated with compressed air, was mounted below the four-bar linkage for rotating the fin rays and the membrane (Supplementary Video S1). The biomimetic spiny dorsal fin has a 92-mm span, 65-mm chord length, and a mass of 47.9 g.

To mimic a single biomimetic fin ray, we used two cylindrical soft actuators positioned symmetrically on the left and right to provide motion at the fin ray's base. Note that the natural soft fin ray possesses a bilaminar structure composed of two half-ray elements (called hemitrichs) (Fig. 2C, E), but we elected to simplify the natural fin ray design by not using a bilaminar structure to reduce the number of fin actuators by a factor of two, and to use single elements to represent each ray to reduce the number of actuators (Fig. 2B, F). Force is applied to a biological fin ray via inclinator muscles attached to the fin base, and a ligament (shown in green) that joins the base of the fin ray slides over a supporting cartilage pad (Fig. 2C). In the bioinspired fin, inflating the soft actuators on each side of the fin ray (up and down) induces the fin ray to move side to side (Fig. 2D; Supplementary Video S2). A flexible arc-shaped hinge,[33] which allows the fin ray to be bent laterally, was placed at a position corresponding to that of the soft ligament of a biological fin ray (inset in Fig. 2D).

We used four pairs of fiber-reinforced soft actuators (eight total) to mimic the dorsal/anal inclinator muscles of four soft rays. We also used one fiber-reinforced soft actuator to produce the erecting/folding motion through a four-bar linkage mechanism, similar to that found in a spiny dorsal fin. The soft dorsal and anal fins are able to perform both the erecting/folding motions and to produce bending side to side (Fig. 2F; Supplementary Video S3). Both the biomimetic soft dorsal and anal fins have a 115-mm span, 74-mm chord length, and a mass of 45.8 g (Fig. 2F). The distance between the trailing dorsal fin margin and the leading edge of the caudal fin is 66.5 mm.

Cylinder-shaped fiber-reinforced soft actuators of two different sizes were fabricated for the fin erect/fold mechanisms (25 mm in length, 19 mm in diameter) and the flapping mechanisms (16 mm in length, 10 mm in diameter). The soft actuators consisted of four components: the inner and outer extendable silicone elastomer layers, Kevlar thread for constraining the radial expansion, a driving end that connects with the mechanism, and a fixed end with a pressure input tube (Supplementary Fig. S1A). All the molds for the casting process were printed using a 3D printer (MakerBot Replicator X5; MakerBot Industries, Inc.). The fabrication process of a fiber-reinforced soft actuator is shown in Supplementary Figure S1B. When pressurized air is applied to the soft actuator, it produces linear motion that generates the erect/fold motion of the fin rays (Fig. 2I). Air pressure was measured using a high-precision digital pressure transducer (ZSE30AF/ISE30A, SMC Corp., Tokyo, Japan).

The computer aided design (CAD) model of the biomimetic fin was then transferred to an Objet Connex500 C3 (Stratasys, Ltd., Eden Prairie, MN), a multimaterial 3D printer, for fabrication. The different mechanical elements of the biomimetic fins were assigned different material stiffnesses represented by different colors (see color bars in Fig. 2F). The rigid fin rays and fin base support (pink) were fabricated from rigid material with a Young's modulus of 3000 Mpa (VeroWhitePlus RGD835). The flexible hinge of each fin ray (gray) was fabricated from flexible material with

Downloaded by Ucsb Libraries University of California Santa Barbara from www.liebertpub.com at 04/10/18. For personal use only.

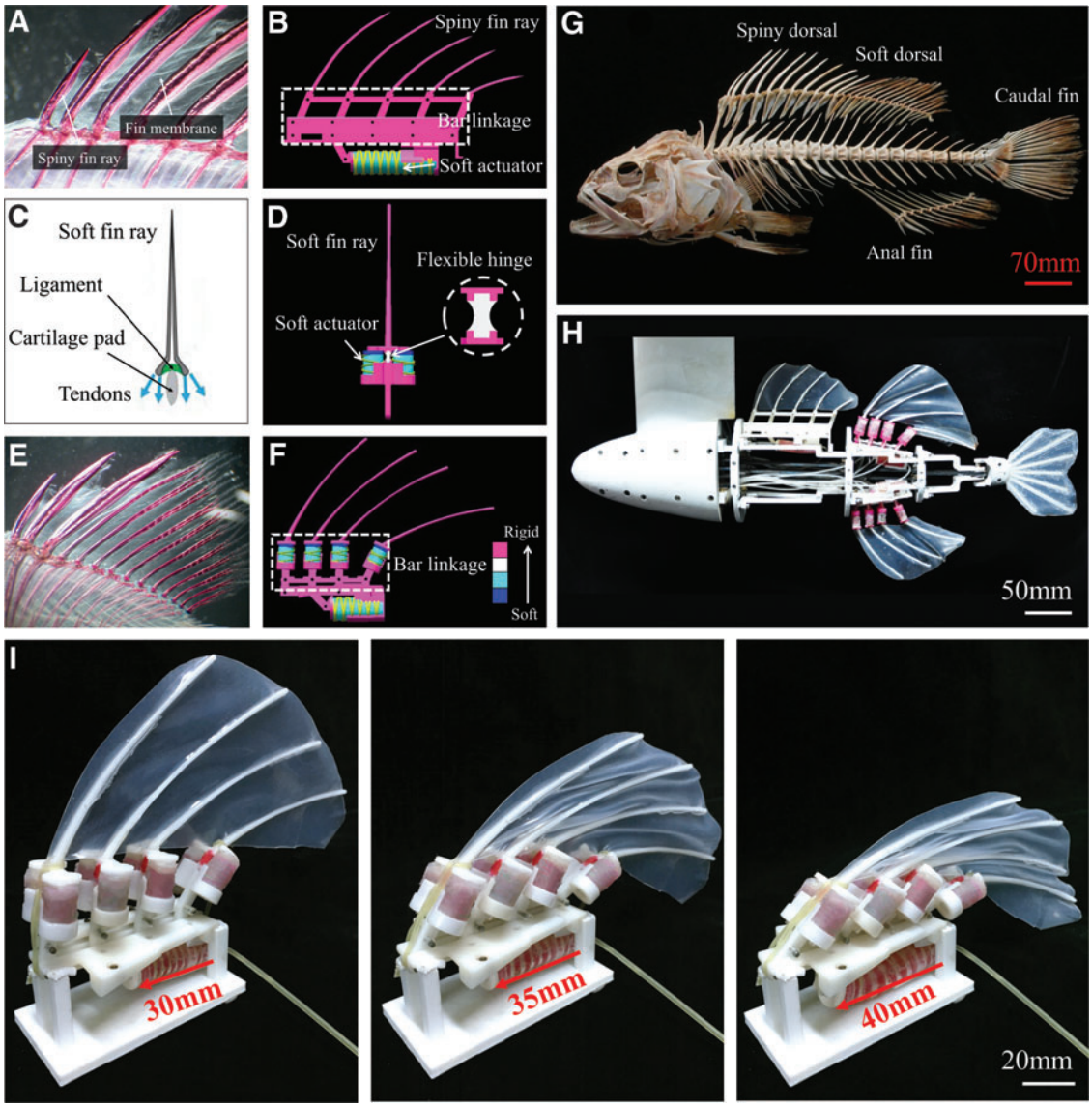

FIG. 2. Morphology of the median fins of bony fishes and the biomimetic prototypes with mechanical elements and mechanisms. **(A)** Image of a cleared and stained spiny dorsal fin in a bluegill sunfish (*Lepomis macrochirus*) with rigid spines (*red*) and the soft fin membrane (*translucent*). **(B)** CAD model of the biomimetic spiny dorsal fin. The bar linkage mechanism for the erect/fold motions, which translates the linear movement of the soft actuator (driven by a pneumatic system) into the rotational movement of the fin. **(C)** Simplified fin ray bending mechanism. Force is applied to a fin ray via inclinator muscles attached through tendons near the base of the fin ray. A ligament (*green*) that attaches to the base of the fin ray slides over a supporting cartilage pad. **(D)** Model of a single biomimetic fin ray. The principal elements of the fin structures were assigned multiple materials represented by different colors. The spines and rays have the largest stiffness (indicated by *red*), the materials in the fin mechanism include fully rigid material (indicated by *red*), and flexible material (indicated by *gray*). Fiber-reinforced soft actuators (indicated by cyan) located on each side allow the fin ray to flap laterally. The material stiffness of the biomimetic fins spans five orders of magnitude, ranging from 0.01 to 3000 Mpa. **(E)** Anal fin in a bluegill sunfish to show the leading spines and posterior flexible rays. **(F)** Model of the soft dorsal fin rays. Fluidic elastomeric soft actuators that mimic the dorsal/anal inclinator, and erector/depressor muscles allow the biomimetic soft fin to erect, fold, and flap laterally. The mechanical assembling process is available in Supplementary Video S4. **(G)** Skeleton of a snowy grouper (*Hyporthodus niveatus*) showing the segmented vertebral column and the major median fins, to illustrate the relative positions of the spiny dorsal, soft dorsal, anal, and caudal fins (scale bar is 70 mm). **(H)** Photograph of the biomimetic robotic fish with all median fins (BL 580 mm; maximum body width 80 mm; maximum body height with fins 230 mm) illustrating the biomimetic spiny dorsal, soft dorsal, and anal fins (scale bar is 50 mm). **(I)** Biomimetic soft dorsal fin at fully erected (pneumatic pressure: 0 Kpa), half-erected (153 Kpa), and fully fold down (278 Kpa) states. CAD, computer aided design. Color images available online at www.liebertpub.com/soro

Downloaded by Ucsb Libraries University of California Santa Barbara from www.liebertpub.com at 04/10/18. For personal use only.

a Young's modulus of 1.1 Mpa (TangoPlus FLX930). The soft actuators were fabricated with silicone elastomer (blue) with a Young's modulus of 0.5 Mpa (DragonSkin 30). The fin membrane, with a thickness of 600 μm, was fabricated by a spin coater (MV300; Marath, Inc.) using a silicone elastomer material (Ecoflex 0010; Smooth-On, Inc.). The membrane was then glued evenly to the fin rays using silicone epoxy.

We programmed the median fins to move according to five typical median fin motion patterns observed in bony fishes during swimming[1,3,4,9,34]: (1) all fins folded down; (2) spiny dorsal fin erect and soft dorsal/anal fins folded down; (3) spiny dorsal fin folded down with soft dorsal/anal fins half-erect; (4) spiny dorsal fin folded down and soft dorsal/anal fins fully erect; and (5) spiny dorsal fin and soft dorsal/anal fins fully erect.

We positioned the biomimetic spiny dorsal, soft dorsal, and soft anal fins on the robot model in locations corresponding to the median fin positions of a typical perciform teleost fish such as a largemouth bass or yellow perch (Fig. 2G; see the assembly process in Supplementary Video S4). This robotic fish body, which has been applied in our previous studies to understand fish undulatory propulsion,[24,30] has four rigid segments that can be actuated independently by servo motors (RE40; Maxon Motor, Inc., Switzerland). The robotic fish body has a total BL of 58.8 cm and mass of 2.79 kg, and has a similar shape to that of a generalized carangiform fish swimmer, whose body undulation is primarily confined to the posterior of the BL.[35] The spiny dorsal fin was mounted posterior to the head of the robot, and the soft dorsal and anal fins were symmetrically mounted on the upper and lower positions of the second segment of the fish body, respectively (Fig. 2H). The four segments of the robotic fish were controlled by a servo motor coordinator (MC206; Trio Motion Technology, United Kingdom) to produce a fish-like undulatory movement. Body kinematics was defined by the following:

$$h(x,t) = \left(c_1 x + c_2 x^2\right) \sin\left(\frac{2\pi}{\lambda} x \pm \frac{2\pi}{f} t\right), \qquad (1)$$

where $h(x,t)$ denotes the displacement along the lateral direction in a body-fixed coordinate system; x denotes the displacement along the main body axis (note: x is measured starting from 1/3L of the robotic fish); L represents the total length of the body; λ denotes the body wave length, which was set to 0.96 BL to mimic carangiform locomotion.[35] f denotes the locomotion frequency, chosen to be 1.5 Hz for this study.

From our live bass trials, the frequency ranges from 1.9 to 4.48 Hz in linear acceleration (0.12–2.07 BL/s^2) and 1.41–3.70 Hz in steady swimming (1–2 BL/s). Frequency range of live fishes was also provided in a recent study on the live fish linear acceleration.[29] According to the biological results, 1.5 Hz is within the biological range of the flapping frequency that is common to slow to moderate freely swimming fishes. c_1 and c_2 were used to control the amplitude of the caudal fin. We use the peak-to-peak oscillation amplitude at the caudal peduncle to define the amplitude (h). From our bass observation (Fig. 1), the peduncle amplitude is within 0.09–0.14 BL in linear acceleration (0.12–2.07 BL/s^2) and 0.07–0.1 for steady swimming (1–2 BL/s). Therefore, we choose to fix the peduncle amplitude to 0.1 BL ($h = 0.1$ BL) as it is the typical biological range of the peduncle amplitude of the live fishes.

The experimental apparatus is constructed as follows (see Fig. 3A for a schematic view): The servo towing system has a travel distance of 7.5 m with a position control accuracy of 0.1 mm. Underneath the towing system is a water tank measuring $7.8 \times 1.2 \times 1.1$ m, in which the robotic fish has sufficient space to move. As Figure 3A shows, a low-drag streamlined strut, which is fixed to a force transducer above the water, penetrates the water and connects to the head of the fish. During experiments, the robotic fish was towed (by the servo towing system) at mid-depth in the tank to avoid interference from the free water surface and the bottom of the tank. The measured transducer forces of the robotic fish were measured using a multiaxis ATI force transducer (mini-40; ATI Industrial, Inc.). As shown in the black dashed box in Figure 3A, when the experimental apparatus was in operation, we were able to simultaneously record force data and digital particle image velocimetry (DPIV) images, control the speed of the carriage, and actuate the robotic fish model. The DPIV system was used to measure the flow field. For more details about the DPIV apparatus, which includes the laser system, high-speed camera, and particles (10 μm average size glass microspheres) to seed the water, refer to our previous article.[24]

One technical issue for the robot was that it needed to be towed through the water from still to steady swimming state to imitate how a fish would naturally move during acceleration. In this article, we used a simple metric, ''critical linear acceleration'' (A_{cla}, unit: m/s^2), to characterize the biorobotic fish's linear acceleration performance under different fin states. This acceleration method is an extension of our previously described self-propelled steady swimming method for fish robotics.[36,37]

The experimental process for realization compromises several steps. Step 1: for each state, we first fixed the robotic fish body motion and then varied the towing speed U until the time-averaged axial force measured by the force transducer was 0 (Fig. 3B). Lauder *et al.*[36] also presented a diagram showing that the robot swims at a self-propelled time-averaged constant speed as a result of a thrust and drag force balance over a single tail beat cycle. Each force is the mean from five repeated trials at each towing speed ($n = 5$). We calculated the self-propelled speed (U_{sps}, which is marked out by the vertical dashed line with label in Fig. 3B) based on the towing speed and the measured axial force based on a previously described method.[30,38,39] Step 2: We program the towing system with different linear acceleration rates. Linear acceleration profiles of the towing system (the colors of the acceleration profiles correspond to those in Fig. 3C) and the axial force/time history during both linear acceleration followed by steady swimming for the black profile. The robotic fish model accelerates from initial zero velocity, and then, we calculated the mean axial forces during the acceleration stage for each acceleration rate. Each force is the mean from five repeated trials at each acceleration rate ($n = 5$).

Data for the mean axial forces generated at acceleration rates are shown in Figure 3C (the A_{cla} is marked out by the vertical dotted line with label). In Figure 3D, we show six different linear acceleration profiles for acquiring the A_{cla} of all fins erected up (case e), which were determined by linearly fitting the mean force data for each acceleration rate (Fig. 3C). The black axial force/time history profile in Figure 3D is the result when robotic fish was first towing at a

Downloaded by Ucsb Libraries University of California Santa Barbara from www.liebertpub.com at 04/10/18. For personal use only.

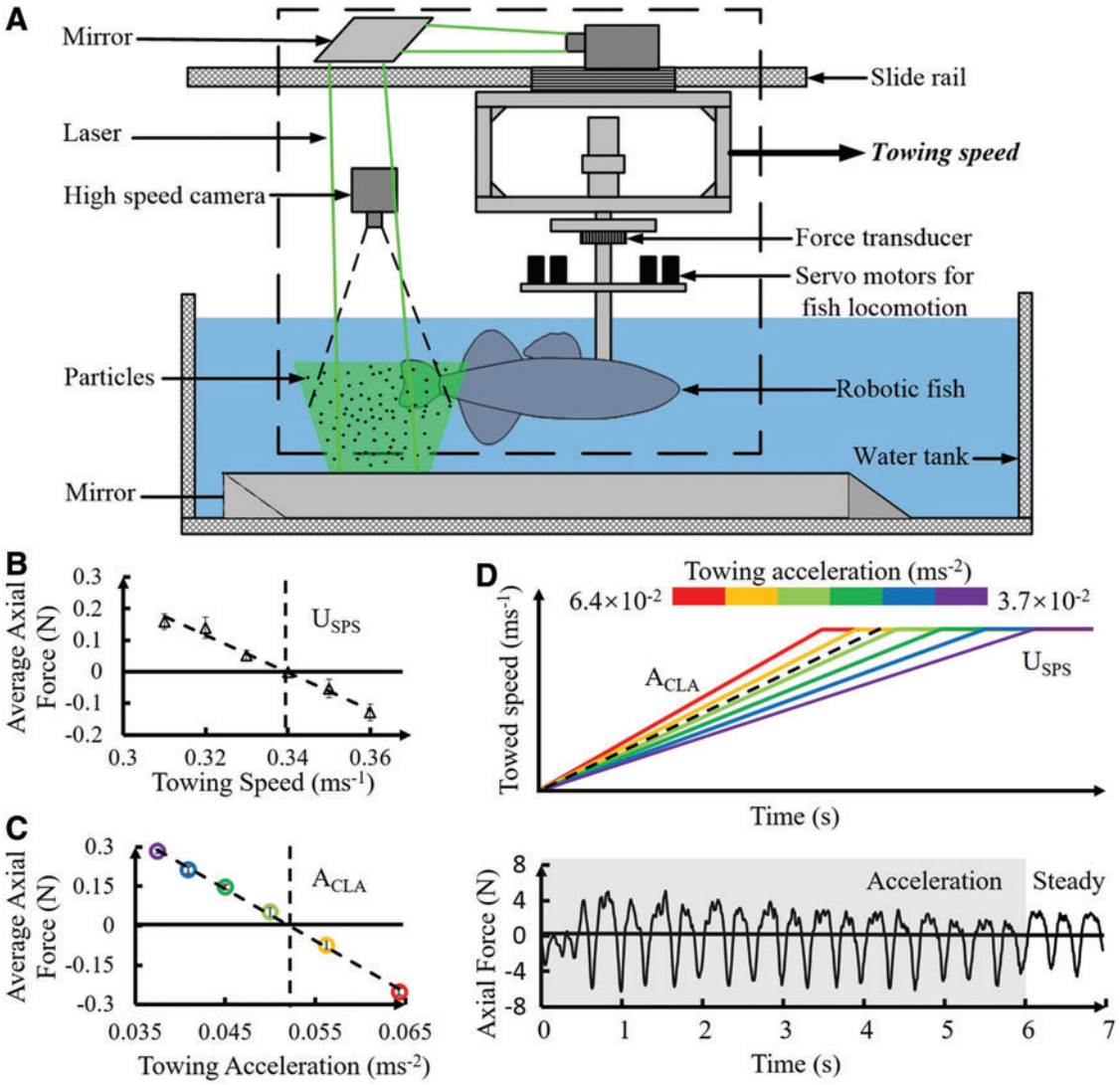

FIG. 3. The hydrodynamic experimental apparatus for testing the biomimetic robotic fish and our approach for evaluating linear acceleration performance. **(A)** Schematic view of the experimental system for the robotic fish model in a flow tank where the water is still. The main mechanical components of the apparatus and the laser system for DPIV are marked. The *x*-axis is along the fish axial length; the *y*-axis is in the lateral direction; and *z* is vertical. The thick *arrow* labeled ''towing speed'' indicates the direction of linear acceleration of the robotic fish. Note that all of the robotic fish's power supply, motion control, amplifier, and data acquisition system were contained within the carriage. **(B)** The towing speed (U) versus the average axial force of the robotic fish in a steady swimming state (kinematics, $h = 0.1$ BL, body wavelength = 0.96 BL, $f = 1.5$ Hz) for acquiring the SPS speed. **(C)** The towing linear acceleration versus the average axial force of robotic fish during linear acceleration for acquiring the critical linear acceleration (see text for discussion). **(D)** Linear acceleration profiles of the towing system (the colors of the acceleration profiles correspond to those in panel (**C**) and the axial force/time history of all fins erected up state (case e) during critical linear acceleration followed by steady swimming for the *black* profile. Error bars are ±1 s.e.m. DPIV, digital particle image velocimetry; s.e.m., standard error of the mean; SPS, self-propelled swimming. Color images available online at www.liebertpub.com/soro

critical linear acceleration state (5.2×10^{-2} m/s^2 (0.09 BL/s^2), gray shaded area) and then the steady swimming state (0.339 m/s). The axial force oscillation of these two states is centered around zero baseline.

Results

Kinematics of the biomimetic robotic fish

The biomimetic spiny dorsal fin can fold down to 45% of its fully erected state at 285 Kpa inflation pressure. The biomimetic soft dorsal and anal fins were able to fully erect at a pneumatic pressure of zero (Fig. 4A), half-erect at a pressure of 304 Kpa (Fig. 4B), and fold down by a 70% area compared to the fully erect state at a pressure of 425 Kpa (Fig. 4C). Each biomimetic fin was independently controlled by the pneumatic system. When fully erected from the fold state, the side area of the soft dorsal/anal fin changed from 66 to 180 mm^2, and the projection area of whole body (on the lateral plane) changed from 669.3 to 782.6 cm^2. The minimum time for folding down the fins from the fully erected state was 0.30 ± 0.05 s

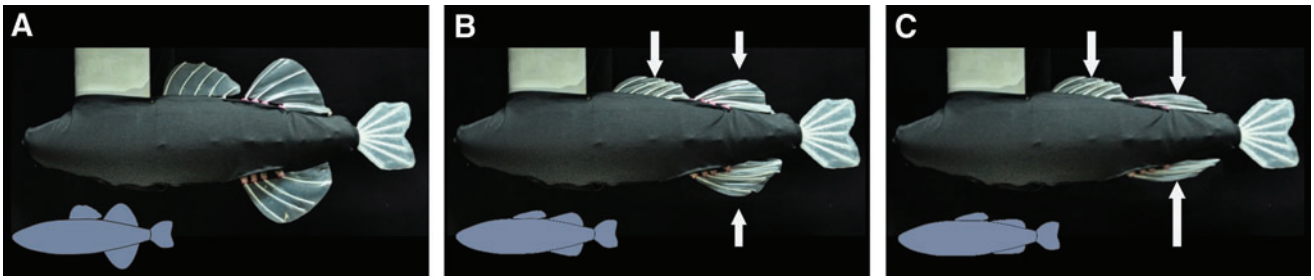

FIG. 4. The robotic fish with median fins. The lateral view of the robotic fish with the biomimetic spiny dorsal, soft dorsal, and soft anal fins **(A)** fully erected, **(B)** half-erected, and **(C)** folded down. The robot was photographed in a static configuration by altering the pneumatic pressure that actuates the fins. The total projected area of the spiny dorsal, soft dorsal/anal fins together (in lateral view) is 180, 113, and 66 cm^2 for fully erected, half-erected, and folded down conditions, respectively. The *white arrows* indicate the direction and magnitude of the folding soft fins. Color images available online at www.liebertpub.com/soro

($n=3$) for the spiny dorsal fin and 0.40 ± 0.05 s ($n=3$) for the soft dorsal/anal fins.

The stiffness variation of the biomimetic soft dorsal/anal fins allows it to withstand impacts from both the axial and lateral directions. In our biomimetic fins, the compliant structures (i.e., the flexible arc-shaped hinge and the soft actuators) allow the fins to deform with obstacles during impact. In Supplementary Video S5, we demonstrate the ability of the fin to deform and then recover from a sudden impact (hit with a 10–mm-diameter rod) occurring under both the still and moving states. As can be seen in Supplementary Video S5, the fin deforms significantly from the impacts in both the lateral and axial directions, but recovers within a short period. During the impact and recovery process, there was no damage to the robot.

The biorobotic model's body and fin kinematic profiles are similar to those of live fish (Fig. 5). A demonstration of the fish body and median fin movements (in air) is available

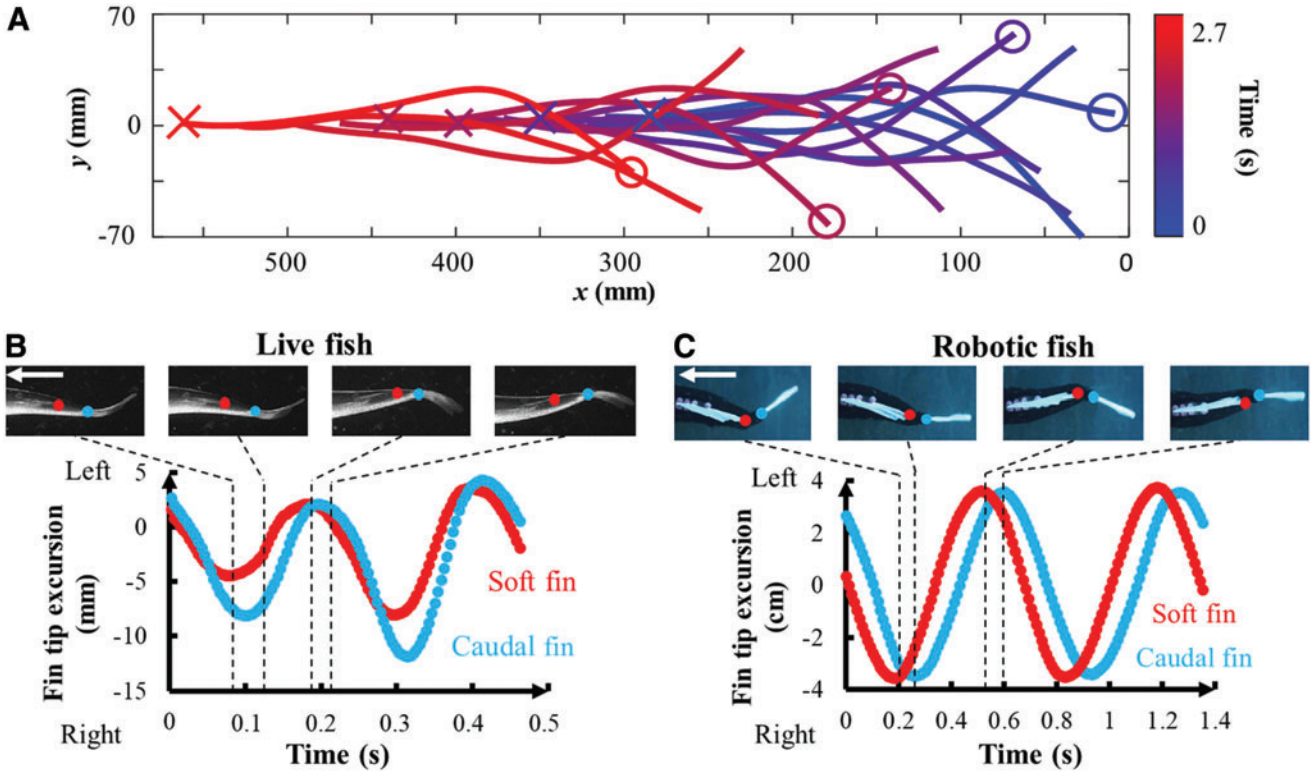

FIG. 5. Kinematics of the robotic fish with median fins. **(A)** The body midline profiles of the robotic fish extracted from three cycles during linear acceleration (0.12 BL/s^2, 0.052 m/s^2). The snout position is indicated by ''x,'' and the tail position is indicated by ''o.'' **(B, C)** Kinematic patterns for the soft dorsal and tail fins oscillating in tandem during linear acceleration for **(B)** a live largemouth bass accelerating at 0.17 BL/s^2 and **(C)** the biomimetic robotic fish accelerating at 0.12 BL/s^2, where BL is the fish BL. Panel **(C)** also includes video images of the two fins moving within a frontal-plane laser sheet over the course of one complete stroke cycle. The *red* point indicates the trailing edge of the soft dorsal fin and the *blue* point indicates the leading edge of the caudal fin. Left–right movements of the trailing edges of the soft dorsal fin and the dorsal lobe of the tail are plotted against time for two consecutive flapping cycles in **(B)** and **(C)**. Color images available online at www.liebertpub.com/soro

Downloaded by Ucsb Libraries University of California Santa Barbara from www.liebertpub.com at 04/10/18. For personal use only.

Downloaded by Ucsb Libraries University of California Santa Barbara from www.liebertpub.com at 04/10/18. For personal use only.

in Supplementary Video S6. A top view of the biorobotic fish's linear acceleration underwater is available in Supplementary Video S7. The robotic fish performed a series of propulsive tail beats with an oscillatory wave traveling along the body, moving the model forward at 0.12 BL/s^2 (Fig. 5A).

The soft dorsal/anal fins moved passively with the body during linear acceleration for both the live fish and the robot. The plots of the marker points on the soft dorsal trailing edge (red) and caudal fin leading edge (blue) over two cycles are provided in Figure 5B, C. For both the soft dorsal and anal fins (in the erect state), the excursions of the marker points display a sinusoidal pattern with an amplitude of 0.07 ± 0.01 BL (10.06 ± 2.03 mm) for the soft dorsal fin and 0.09 ± 0.02 BL (13.85 ± 3.68 mm) for the caudal fin (mean from five repeated trials, $n = 5$). For linear acceleration in the live fish, the observed phase shift between the soft dorsal fin trailing edge and the caudal fin leading edge was 0.10 T (Fig. 5B). By programming the robotic fish body, we obtained a similar phase shift of 0.11 T between the two marker points of the swimming robot (Fig. 5C).

Linear acceleration of the biorobotic fish under varying median fin states

We investigated the effects of the spiny dorsal, soft dorsal, and soft anal fins on the swimming performance of the biorobotic fish under five median fin states (Fig. 6). We found that the soft dorsal/anal fins significantly enhanced both the linear acceleration and the steady swimming speed. With all fins folded down (case a, the control, purple bar), the self-propelled swimming speed (U_{sps}) was 0.329 ± 0.001 m/s (mean ± 1 standard error of the mean). Statistical analysis showed no significant difference in U_{sps} between the erected spiny dorsal fin state (case b, blue bar) and the control ($U_{sps} = 0.329 \pm 0.002$ m/s, analysis of variance [ANOVA], d.f. $= 8$, $p = 0.9057$). When the soft dorsal and anal fins were fully erected (case e, red bar), U_{sps} ($U_{sps} = 0.339 \pm 0.001$ m/s) showed a significant increase of 3.04% (ANOVA, d.f. $= 8$, $p < 0.0001$) over the control case (case a). Notably, the half-erected soft fins (case c, green bar) resulted in the maximum increase in U_{sps} (0.353 ± 0.001 m/s) over the control of 7.29% (ANOVA, d.f. $= 8$, $p < 0.0001$).

In terms of linear acceleration, the critical linear acceleration (A_{cla}) with the spiny dorsal and both the soft fins folded (case a, the control) generated an A_{cla} of 0.040 ± 0.0001 m/s^2, 0.069 BL/s^2). Our statistical analysis showed no significant difference in A_{cla} with the spiny dorsal fin erected ($A_{cla} = 0.040 \pm 0.001$ m/s^2, case b) and the control (ANOVA, d.f. $= 8$, $p = 0.0701$). Erecting the soft fins, however, resulted in significantly faster linear acceleration. For example, with the soft dorsal and anal fins erected and the spiny dorsal folded down ($A_{cla} = 0.053 \pm 0.0001$ m/s^2, 0.091 BL/s^2), case d, yellow bar), a 32.5% greater linear acceleration over the control was generated (ANOVA, d.f. $= 8$, $p < 0.0001$).

The axial force, including the data gathered under non-self-propelled or noncritical linear acceleration conditions used for acquiring the self-propelled swimming speeds and the critical linear accelerations, is also provided (Fig. 6B, D). In most cases, a larger U_{sps} or A_{cla} led to greater axial forces across all flow speeds and linear accelerations tested. The only more complex pattern (Fig. 6B) was observed for the spiny dorsal fin folded (case d) versus erected (case e). With

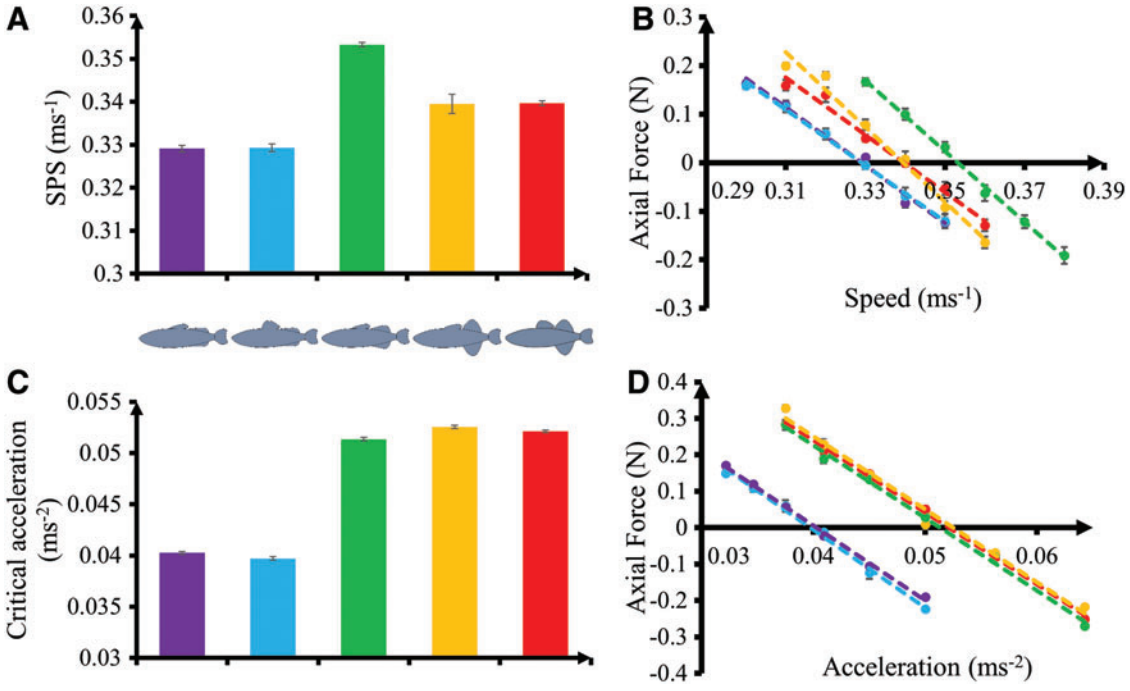

FIG. 6. Swimming performance metrics for the biorobotic fish with different median fin states. Biorobotic fish body kinematics was programmed as $h = 0.1$ BL, body wavelength $= 0.9$ 6 BL, and $f = 1.5$ Hz. **(A)** Self-propelling swimming speeds U_{sps}. **(B)** Axial force on the swimming robotic fish during steady swimming, where the x-axis crossing denotes U_{sps}. **(C)** Critical linear acceleration. **(D)** Axial force on the robotic fish during linear acceleration, where the x-axis crossing denotes the critical linear acceleration. All the axial forces are means from $n = 5$ trials. Error bars are ± 1 s.e.m. Color images available online at www.liebertpub.com/soro

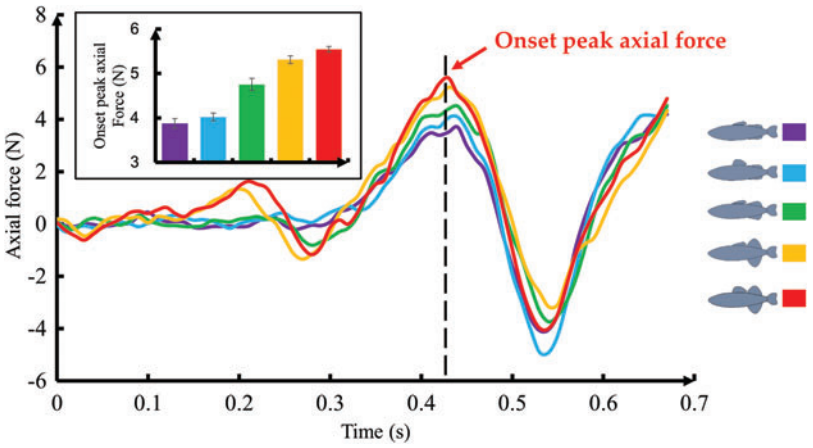

FIG. 7. The measured axial force during the onset stage of linear acceleration (first flapping cycle). Robotic fish body kinematics was programmed as $h = 0.1$ BL, body wavelength = 0.96 BL, and $f = 1.5$ Hz. The *inset panel* shows the maximum force under different fin states. All of the onset peak axial forces are means from $n = 5$ trials. Error bars are ±1 s.e.m. Color images available online at www.liebertpub.com/soro

the spiny dorsal fin erected (case e), the robot experienced higher axial forces when the towing flow speeds were higher than the self-propelled swimming speed (i.e., $U > U_{sps}$). The axial forces on the robotic fish with spiny fin folded (case d) surpassed those with the spiny fin erect (case e) when $U > U_{sps}$.

Total measured forces

We found that median fins can enhance axial force produced by the biomimetic robotic fish during the initial acceleration stage. Figure 7 shows the comparison of the force/time history during the first flapping cycle (the onset stage). The largest difference in forces occurs at the maximum peak of the force curve; the means of the maximum force peaks are provided in the inset panel of Figure 7. We found that (1) erecting the spiny dorsal fin (4.02 ± 0.09 N, case b) increased peak axial force by 3.61% over the control case (3.88 ± 0.11 N, case a); (2) half-erecting the soft dorsal/anal fins (4.75 ± 0.14 N, case c) increased peak axial force by 22.42% over the control; (3) fully erecting the soft fins while folding the spiny fin (5.31 ± 0.08 N, case d) increased peak axial force by 36.86% over the control; and (4) erecting all the fins (5.55 ± 0.06 N, case e) increased peak axial force by 43.04% over the control. The discrepancy in peak axial forces between the cases with erected and folded soft fins is quite large (about 1.5 N), but was negligible between the cases with an erected and folded spiny fin (ANOVA, d.f. = 8, $p = 0.3608$). This indicates that during the onset stage, erected soft dorsal and anal fins contribute significantly to the onset of the measured forces, while the spiny dorsal fin contributes little.

Surprisingly, we found that up to 24.8% of the magnitude of the side force (y-force) on the robotic swimmer was reduced by erecting the soft dorsal/anal fins. Figure 8 shows the side force/time history for two flapping cycles for each fin state during linear acceleration. The force history during steady swimming, although not shown, also demonstrates that the side force was significantly reduced by erecting the soft fins. Erecting the spiny dorsal fin alone (case b, 6.1 ± 0.50 N) did not significantly reduce the magnitude of the side force compared to the control (case a, 6.6 ± 0.39 N; ANOVA, d.f. = 8, $p = 0.11$). Half-erecting the soft dorsal and anal fins (5.7 ± 0.24 N, case c) reduced the magnitude of the force by 13.4% (ANOVA, d.f. = 8, $p = 0.02$) compared to the control. Fully erecting the soft fins while folding the dorsal fin (5.15 ± 0.19 N, case d) reduced the force by 22.2% compared to the control (ANOVA, d.f. = 8, $p = 0.0005$). And when the spiny and both soft fins were erected (4.98 ± 0.28 N, case e), the magnitude of the force was reduced by 24.7% compared to the control (ANOVA, d.f. = 8, $p = 0.0011$).

The instantaneous side force histories of the control (case a), half-erect (case c), and fully erect (case e) fin states are shown in Figure 8B, making the differences in side forces created by different fin states easier to discern. Our results indicate that erecting both the soft dorsal/anal fins and the spiny fin significantly reduces the magnitude of the side forces experienced by the fish robot body, which may in turn reduce yaw motion for the robotic swimmer.

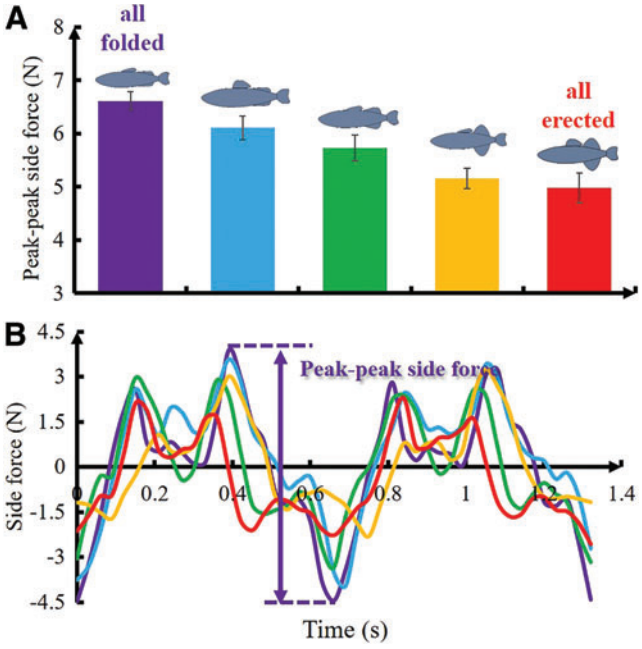

FIG. 8. Peak-to-peak side force on the biorobotic fish during critical linear acceleration. **(A)** The average peak-to-peak side forces on the biorobotic fish under different median fin states. **(B)** The instantaneous side force for two flapping cycles. The *purple double arrow* indicates the magnitude of the peak-to-peak side force with no erect fins. Note that the robotic fish is swimming at the critical linear acceleration state. Error bars are ±1 s.e.m. Color images available online at www.liebertpub.com/soro

Downloaded by Ucsb Libraries University of California Santa Barbara from www.liebertpub.com at 04/10/18. For personal use only.

Wake flow patterns

We found that lateral flows generated by the soft dorsal and the caudal fin were oriented to opposite sides and reduced the magnitude of the overall side forces during both linear acceleration and steady swimming. The difference in the transducer forces is the result of different momentum transfers from the robotic swimmer to the water. Figure 9 shows the midfin flow field of the soft dorsal fin visualized using velocity vectors and vorticity contours. Wake flow patterns were investigated to identify the reasons for the observed differences in the axial forces and side forces. Wake flows produced by bluegill sunfish, a perciform teleost species with a spiny and soft dorsal fin, are provided in Figure 9A, B; we found that the wake flows generated by the robot (Fig. 9C, D) are similar to that of the live fish.

For the erected soft dorsal/anal fins (case e) and the control state, fluid jets have been identified between the soft dorsal fin and the caudal fin during linear acceleration. The direction of the jet produced by the soft dorsal fin has a jet angle of 15.6° (relative to a horizontal or mediolateral direction), reduces the momentum in the x-direction, and may lead to lower forces in the lateral direction (Fig. 9C). The caudal fin wake has an angle of 10.6° (relative to the horizontal line), but in the opposite direction to that of soft dorsal fin jet (with an angle of 15.6°) (Fig. 9C). The lateral momentum of the caudal fin jet is therefore mostly canceled by the momentum produced by the soft dorsal fin in the opposite lateral direction, thus creating much less overall lateral flow velocity compared with the control case (Fig. 9D). This is in agreement with the side force measurement results in Figure 8. A time series of wake flow produced by the soft dorsal fin and caudal fin of the robotic fish during one entire stroke during the linear acceleration is provided in Supplementary Figure S2.

Swimming speed varies with time throughout a linear acceleration, and the wake flow is not periodic. Figure 10 shows a series of representative flow fields during a critical linear acceleration of the robotic swimmer, starting from 0 m/s and reaching a steady swimming speed of 0.3 m/s (A_{cla} = 0.05 m/s^2, 0.086 BL/s^2). The caudal fin flow fields were visualized using velocity vectors. During linear acceleration, the caudal fin wake showed a typical fish-like pair of counter-rotating vortices shed per tail stroke (Fig. 10A–D). The energy transfer between the caudal fins was assessed through the momentum and the jet angle (averaged from eight cycles) over time

Downloaded by Ucsb Libraries University of California Santa Barbara from www.liebertpub.com at 04/10/18. For personal use only.

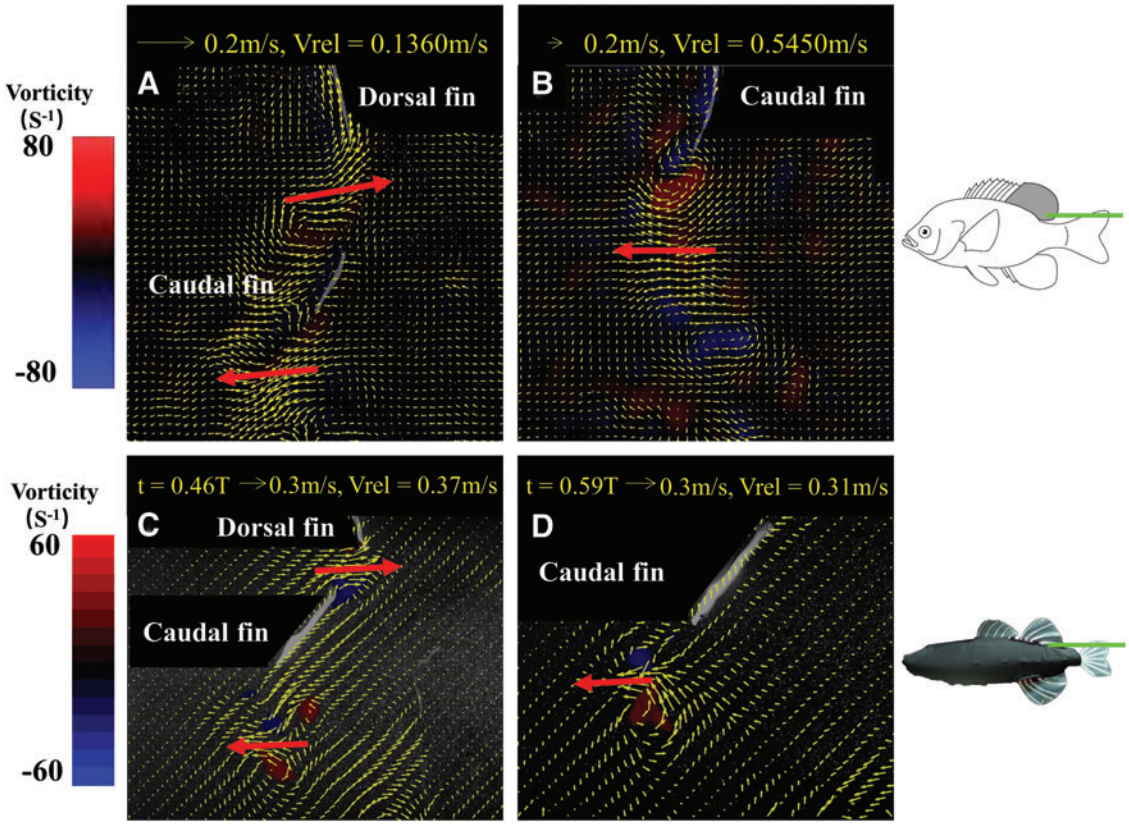

FIG. 9. Wake flows generated by the soft dorsal fin and caudal fin of a bluegill sunfish and the robotic fish during linear acceleration (0.052 m/s^2). **(A)** The wake flow around the dorsal and caudal fins in a bluegill sunfish (*Lepomis macrochirus*) with soft dorsal fins erect. The lateral jet produced by the dorsal fin acts in the opposite direction to that of the caudal fin (*red arrows*). **(B)** The wake flow behind the bluegill sunfish caudal fin to show the lateral jet flows produced by the tail. **(C)** The velocity field of the biorobotic fish with its soft dorsal and anal fins erect (t = 0.53T, when the maximum tail-beat speed occurs). The dorsal fin produced a lateral jet in the opposite direction to that of the caudal fin. **(D)** The wake flow of the robotic model with all median fins folded down (t = 0.53T, when the maximum tail-beat speed happens). The direction of the jet (*red*) is also labeled in both C and D. Background flow velocities (V_{rel}) have been subtracted for the velocity vectors of both the fish and robot. Color images available online at www.liebertpub.com/soro

Downloaded by Ucsb Libraries University of California Santa Barbara from www.liebertpub.com at 04/10/18. For personal use only.

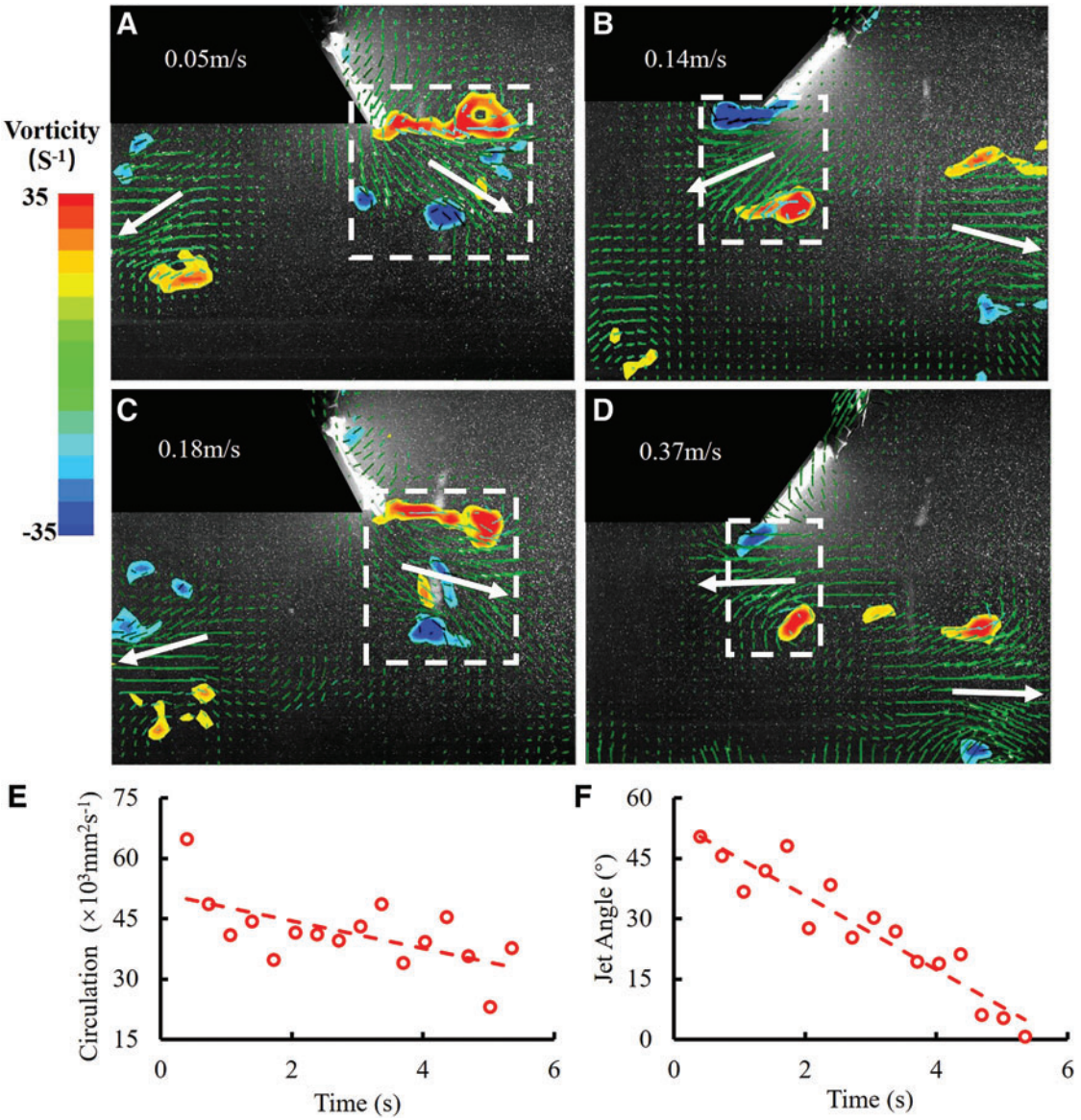

FIG. 10. Time series **(A–D)** of DPIV wake flow images behind the biorobotic fish's caudal fin at a linear acceleration of 0.052 m/s^2. The laser light sheet was aligned with the middle of the caudal fin. The vortex pair that we used to calculate the circulation was marked according to the *white dashed box* in each figure panel. The jet angles are labeled relative to the horizontal with *white arrows*. The instantaneous vorticity during linear acceleration is marked according to the colored panel. **(E)** The circulation of vortices versus time during linear acceleration. The vortex circulation values were calculated from the time instant when the caudal fin has reached its maximum flapping position to the side (as the time instant shown in **A–D**). The vortex marked by the *white dashed box* in each panel was used to calculate the circulation and the jet angle. **(F)** Jet angle of the wake flow versus time during linear acceleration. Color images available online at www.liebertpub.com/soro

(Fig. 10E, F). The two metrics reached their maximum at the initial flap ($t = 1.06$ s), and the momentum and jet angle decrease with the flow speed during linear acceleration. Wake vortex circulation dropped from 64,786 to 37,830 mm^2/s by the end of linear acceleration ($t = 5.35$ s), with the jet angle moving laterally and almost parallel to the x-axis.

Discussion

In this study, we designed and fabricated a bioinspired robotic fish with multimaterial spiny dorsal, soft dorsal, and soft anal fins modeled on the morphology and kinematics of bony fishes.[9,34,38] Increasingly, robotics research has emphasized bioinspired designs and mechanisms that examine morphing capabilities in flight[40,41] and the terrestrial locomotion,[42,43] but very few studies have reported on underwater morphing bioinspired robots. Fabricating and actuating biomimetic fins offer several attractive advantages, including the convenience of mimicking diverse fin states and the erecting/folding kinematics of live fish during swimming. It also provides a scientific platform for investigating the hydrodynamic function of median fins. Based on our experimental results, we regard the use of biomimetic median fins as an efficient method for enhancing the swimming performance of underwater biorobots that may inspire smart morphing structures for future underwater robots.[38]

Downloaded by Ucsb Libraries University of California Santa Barbara from www.liebertpub.com at 04/10/18. For personal use only.

Using multimaterial 3D printing to fabricate the fins allowed components to vary considerably in terms of biologically relevant characteristics, including having a Young's modulus ranging from soft (1 Mpa, e.g., the flexible hinge) to very rigid (3 Gpa, e.g., the spiny ray). Fabricating a soft biomimetic fin that can erect/fold and flap laterally was a technical challenge (Fig. 2D). This complex morphology and intrinsic flexibility are a distinctive characteristic of the natural fin of the teleost fishes[1,38] and could not be easily reproduced with traditional mechanical fabrication processes, which led us to use multimaterial 3D printing. Our fabrication and assembling process (Supplementary Video S4) also enable rapid design iteration with little additional cost to change morphological features such as the size, shape, and mechanical stiffness of the fin components, as well as the fin positions on the fish body.[9] Such a modular and modifiable system holds great potential as a scientific tool to examine the locomotor functions of the diverse fin morphologies and kinematic patterns of the different swimming behaviors of bony fishes, including linear acceleration, steady swimming, and burst and coast.

An additional benefit of this design is, in particular, the flexible hinge and soft actuators at each fin base, permitting the soft fins to recover from external impacts without damage (Supplementary Video S5). This demonstrates the potential use of these biomimetic fins for future underwater bioinspired robots near the river bottom or the seafloor, or where obstacles may interfere with a robot's navigation.

Although shape morphing of dorsal and anal fins plays a significant role for fish during swimming,[11,17,34,44] such actively controlled shape changes have not been previously explored in fish-like robotic systems. It was observed that, during the onset stage of linear acceleration (Fig. 7), erecting the soft/anal fins increased the axial force by 43.0% compared to the control pattern (all fins folded). This increase helps accelerate the robotic fish in the x direction at the initial stage.

We also show that erecting the soft dorsal/anal fins played a significant role in linear acceleration (up to 32.5%). In comparison, the effect of erecting the spiny dorsal fin was less important (<3%). Considering the effect of fin area change, and using the control state as a benchmark, we found that the self-propelled swimming speed (U_{sps}) increased even more (7.3%) when the soft dorsal/anal fins were half-erected than when fully erected (3.09%). This is in line with previous studies on the effect of fin use in live fish; for example, decreased fin areas were observed in bluegill sunfish (*Lepomis macrochirus*) at increased flow speeds in a steady swimming state.[9,34] This result suggests that the adjustments made by live fish to median fin area as swimming speed increases may act to increase thrust.

For most fishes, the soft dorsal fin is an active thrust-generating fin at slow to moderate speeds, and accelerates fluid toward the tail.[7,45] However, the role of median fins changes as swimming speed increases. Depending on the magnitude of the imposed acceleration, the median fins could result in either a wake deficit or added momentum. For example, the wake behind the robotic median fins will change substantially as the towing acceleration moves from the red to the purple curves in Figure 3D. Reduced surface area results in both lower added thrust force and lower drag due to reduced surface area. It is difficult to separate these functions as both change together as steady swimming speed increases. Therefore, the reduction in fin area as speed increases may reflect a compromise between the need to reduce drag incurred by the increased fin area and additional thrust due to median fin side-to-side oscillation. Currently, the median fin active oscillations were not taken into account, and this is an important area for future research although challenging because it would require complex additional control of the fin motions.

The projected fin area does change during different cruising velocities and during the acceleration. For example, Standen and Lauder quantified dorsal and anal fin areas over a range of cruising swimming speeds,[9,10] and Tytell *et al.*[11] also compared dorsal function between acceleration and cruising locomotion. It is certainly possible that erecting the dorsal fin will provide more thrust but need more power, but most fishes reduce the dorsal fin area as speed increases. Therefore, there may not exist a specific fin configuration to optimize all swimming metrics (i.e., steady swimming speed, acceleration, and cost-of-transport). However, there may exist multiple fin configurations, and selection of the appropriate one depends on the particular locomotor task. Although we have not measured the power consumption of the robot in this article, investigating the power consumption and the cost-of-transport would be certainly be interesting for future studies.

In this study, we would also like to suggest a new hypothesis about dorsal fin function. Reducing dorsal fin area during acceleration behavior may function not only to reduce drag but it may allow increased yaw (side to side) motion of the anterior body as well, increasing thrust. The erect first dorsal fin will act to increase resistance to yaw of the anterior body, and decreasing dorsal fin area will allow increased body yaw. This increase in yaw is associated with an increase in thrust generation due to changing patterns of pressure over the surface and the presence of a suction zone anteriorly.[29] Modulation of dorsal fin area may thus be associated with multiple functions during fish locomotion.

We were surprised to discover that erecting the biomimetic dorsal/anal fins can also decrease the peak to peak magnitude of the lateral force (y-axis) by 24.8% during linear acceleration, and by 19.5% during steady swimming. The lateral force produced by the dorsal/anal fins counteracted the caudal fin force because the motion of these two groups of fins is largely out of phase. Flow visualization of fin wake pattern results showed that this reduction in side force amplitude is most likely due to the production of counteracting momentum jets: the dorsal and anal fins generate momentum to the opposite side as momentum produced by the caudal fin. This result suggests a new hypothesis for the function of dorsal and anal median fins in fishes: reduction of yaw moments. This point was also demonstrated in a recent computational fluid dynamic study,[46] and the increased head yaw as speed increases and during acceleration.[29]

Undulatory locomotion of a flexible body necessarily generates large side forces, and analyses of wake flow patterns in freely swimming fishes have shown that lateral forces generated by the tail and body alone can be twice that of the thrust force produced.[45,47] Recoil from the large oscillatory lateral forces produced by the oscillating tail will generate yaw moments that increase drag and the cost of locomotion. However, the presence of median fins such as the dorsal and anal that are under active control allows fish to use these fins to generate oppositely signed torques to greatly reduce the effect of lateral forces produced at the tail. This hypothesis remains to be tested

by experiments on live fish, but is an intriguing notion that emerges from analysis of forces produced by our biomimetic fish robotic system with morphing median fins.

It should be noted that our current robotic model did not take into account the dynamic tail beat changing frequency or amplitude and how this changes during different acceleration values. We also did not study acceleration compared to steady swimming and alter the kinematics of the model in the way that fish do.[29] Modulating the tail beat frequency to accelerate the robotic fish is an interesting direction for future study.

We also found that the orientation and circulation of the caudal fin wake differed substantially during linear acceleration compared to steady swimming (Fig. 10). Tytell[12] conducted the most comprehensive analysis to date of wake flows during acceleratory locomotion. His study reported wake flow of eels (*A. rostrata*) during linear acceleration and he noted that the caudal momentum jets were oriented in a more downstream/streamwise direction, with the addition of axial momentum relative to steady swimming wake flows. We have observed a similar phenomenon in our biorobotic fish, suggesting that the addition of axial wake momentum is necessary to achieve changes in swimming velocity.

Downloaded by Ucsb Libraries University of California Santa Barbara from www.liebertpub.com at 04/10/18. For personal use only.

Acknowledgments

The authors thank Zheyuan Gong for his contribution to the help of the pneumatic control system of the median fins. This work was supported by the National Science Foundation support projects, China (Grant Nos. 61403012, 61633004, and 61333016), and the Office of Naval Research grant ONR N00014-0910352 to G.V.L.

Author Disclosure Statement

No competing financial interests exist.

References

1. Jayne BC, Lozada AF, Lauder GV. Function of the dorsal fin in bluegill sunfish: motor patterns during four distinct locomotor behaviors. J Morphol 1996;228:307–326.
2. Lauder GV, Nauen JC, Drucker EG. Experimental hydrodynamics and evolution: function of median fins in ray-finned fishes. Integr Comp Biol 2002;42:1009–1017.
3. Chadwell BA, Standen EM, Lauder GV, Ashley-Rossn MA. Median fin function during the escape response of bluegill sunfish (*Lepomis macrochirus*). I: Fin-ray orientation and movement. J Exp Biol 2012;215:2869–2880.
4. Chadwell BA, Standen EM, Lauder GV, Ashley-Ross MA. Median fin function during the escape response of bluegill sunfish (*Lepomis macrochirus*). II: Fin-ray curvature. J Exp Biol 2012;215:2881–2890.
5. Tytell ED. Median fin function in bluegill sunfish *Lepomis macrochirus*: streamwise vortex structure during steady swimming. J Exp Biol 2006;209:1516–1534.
6. Maia A, Wilga CA. Function of dorsal fins in bamboo shark during steady swimming. Zoology 2013;116:224–231.
7. Maia A, Lauder GV, Wilga CD. Hydrodynamic function of dorsal fins in spiny dogfish and bamboo sharks during steady swimming. J Exp Biol 2017;220:3967–3975.
8. Lauder GV, Drucker EG. Morphology and experimental hydrodynamics of fish fin control surfaces. IEEE J Oceanic Eng 2004;29:556–571.
9. Standen EM, Lauder GV. Dorsal and anal fin function in bluegill sunfish *Lepomis macrochirus*: three-dimensional kinematics during propulsion and maneuvering. J Exp Biol 2005;208:2753–2763.
10. Standen EM, Lauder GV. Hydrodynamic function of dorsal and anal fins in brook trout (*Salvelinus fontinalis*). J Exp Biol 2007;210:325–339.
11. Tytell ED, Standen EM, Lauder GV. Escaping flatland: three-dimensional kinematics and hydrodynamics of median fins in fishes. J Exp Biol 2008;211:187–195.
12. Tytell ED. Kinematics and hydrodynamics of linear acceleration in eels, *Anguilla rostrata*. P Roy Soc Lond B Bio 2004;271:2535–2540.
13. Videler JJ, Weihs D. Energetic advantages of burst-and-coast swimming of fish at high speeds. J Exp Biol 1982;97:169–178.
14. Wu G, Yang Y, Zeng L. Kinematics, hydrodynamics and energetic advantages of burst-and-coast swimming of koi carps (*Cyprinus carpio koi*). J Exp Biol 2007;210:2181–2191.
15. Domenici P, Blake R. The kinematics and performance of fish fast-start swimming. J Exp Biol 1997;200:1165–1178.
16. Alben S, Witt C, Baker TV, Anderson E, Lauder GV. Dynamics of freely swimming flexible foils. Phys Fluids 2012;24:051901.
17. Borazjani I. The functional role of caudal and anal/dorsal fins during the C-start of a bluegill sunfish. J Exp Biol 2013;216:1658–1669.
18. Rus D, Tolley MT. Design, fabrication and control of soft robots. Nature 2015;521:467–475.
19. Liu H, Taylor B, Curet O. Fin ray stiffness and fin morphology control ribbon-fin-based propulsion. Soft Robot 2017;4:103–116.
20. Long Jr JH, Combes S, Nawroth J, Hale M, Lauder GV, Swartz S, *et al.* How does soft robotics drive research in animal locomotion? Soft Robot 2014;1:161–168.
21. Lauder GV. Flexible fins and fin rays as key transformations in ray-finned fishes. In Dial KP, Shubin N, Brainerd EL (Eds). Great Transformations in Vertebrate Evolution. Chicago: University of Chicago Press, 2015, p. 31.
22. Tangorra JL, Lauder GV, Hunter IW, Mittal R, Madden PG, Bozkurttas M. The effect of fin ray flexural rigidity on the propulsive forces generated by a biorobotic fish pectoral fin. J Exp Biol 2010;213:4043–4054.
23. Esposito CJ, Tangorra JL, Flammang BE, Lauder GV. A robotic fish caudal fin: effects of stiffness and motor program on locomotor performance. J Exp Biol 2012;215:56–67.
24. Wen L, Wang T, Wu G, Liang J, Wang C. Novel method for the modeling and control investigation of efficient swimming for robotic fish. IEEE T Ind Electron 2012;59:3176–3188.
25. Marchese AD, Onal CD, Rus D. Autonomous soft robotic fish capable of escape maneuvers using fluidic elastomer actuators. Soft Robot 2014;1:75–87.
26. Kim HS, Lee JY, Chu WS, Ahn SH. Design and fabrication of soft morphing ray propulsor: undulator and oscillator. Soft Robot 2017;4:49–60.
27. Jusufi A, Vogt DM, Wood RJ, Lauder GV. Undulatory swimming performance and body stiffness modulation in a soft robotic fish-inspired physical model. Soft Robot 2017;4:202–210.
28. Tangorra J, Phelan C, Esposito C, Lauder GV. Use of biorobotic models of highly deformable fins for studying

the mechanics and control of fin forces in fishes. 2011;51: 176–189.
29. Akanyeti O, Putney J, Yanagitsuru YR, Lauder GV, Stewart WJ, Liao JC. Accelerating fishes increase propulsive efficiency by modulating vortex ring geometry. Proc Natl Acad Sci USA 2017;52:13828–13833.
30. Wen L, Wang T, Wu G, Liang J. Quantitative thrust efficiency of a self-propulsive robotic fish: experimental method and hydrodynamic investigation. IEEE-ASME T Mech 2013; 18:1027–1038.
31. Ren Z, Yang X, Wang T, Wen L. Hydrodynamics of a robotic fish tail: effects of the caudal peduncle, fin ray motions and the flow speed. Bioinspir Biomim 2016;11:016008.
32. Jayne BC, Lauder GV. Speed effects on midline kinematics during steady undulatory swimming of largemouth bass, *Micropterus salmoides*. J Exp Biol 1995;198:585–602.
33. Chen H. Analysis of the rigidity of arc flexible hinge with different geometrical parameters. International Conference on Computer and Computing Technologies in Agriculture, Springer, Berlin, Heidelberg, 2011, pp. 195–200.
34. Drucker EG, Lauder GV. Locomotor function of the dorsal fin in rainbow trout: kinematic patterns and hydrodynamic forces. J Exp Biol 2005;208:4479–4494.
35. Sfakiotakis M, Lane DM, Davies JBC. Review of fish swimming modes for aquatic locomotion. IEEE J Oceanic Eng 1999;24:237–252.
36. Lauder GV, Anderson EJ, Tangorra J, Madden PG. Fish biorobotics: kinematics and hydrodynamics of self-propulsion[J]. J Exp Biol 2007;210:2767–2780.
37. Wen L, Lauder G. Understanding undulatory locomotion in fishes using an inertia-compensated flapping foil robotic device[J]. Bioinspir Biomim 2013;8:046013.
38. Lauder GV, Lim J, Shelton R, Witt C, Anderson E, Tangorra JL. Robotic models for studying undulatory locomotion in fishes. Mar Technol Soc J 2011;45:41–55.
39. Wen L, Weaver JC, Lauder GV. Biomimetic shark skin: design, fabrication and hydrodynamic function. J Exp Biol 2014;217:1656–1666.
40. Stowers AK, Lentink D. Folding in and out: passive morphing in flapping wings. Bioinspir Biomim 2015;10: 025001.
41. Jenett B, Calisch S, Cellucci D, Cramer N, Gershenfeld N, Swei S, *et al.* Digital morphing wing: active wing shaping concept using composite lattice-based cellular structures. Soft Robot 2017;4:33–48.
42. Lin HT, Leisk GG, Trimmer B. GoQBot: a caterpillar-inspired soft-bodied rolling robot. Bioinspir Biomim 2011; 6:026007.
43. Felton S, Tolley M, Demaine E, Rus D, Wood RJ. A method for building self-folding machines. Science 2014; 345:644–646.
44. Shih AM, Mendelson L, Techet AH. Archer fish jumping prey capture: kinematics and hydrodynamics. J Exp Biol 2017;220:1411–1422.
45. Drucker EG, Lauder GV. A hydrodynamic analysis of fish swimming speed: wake structure and locomotor force in slow and fast labriform swimmers. J Exp Biol 2000;203: 2379–2393.
46. Liu G, Ren Y, Dong H, Akanyeti O, Liao JC, Lauder GV. Computational analysis of vortex dynamics and performance enhancement due to body–fin and fin–fin interactions in fish-like locomotion. J Fluid Mech 2017;829:65–88.
47. Nauen JC, Lauder GV. Hydrodynamics of caudal fin locomotion by chub mackerel, *Scomber japonicus* (Scombridae). J Exp Biol 2002;205:1709–1724.

Address correspondence to:
Li Wen
School of Mechanical Engineering and Automation
Beihang University
Beijing 100191
China

E-mail: liwen@buaa.edu.cn

George V. Lauder
The Museum of Comparative Zoology
Harvard University
Cambridge, MA 02138

E-mail: glauder@oeb.harvard.edu

Downloaded by Ucsb Libraries University of California Santa Barbara from www.liebertpub.com at 04/10/18. For personal use only.